Pyridine-Decorated Carbon Nanotubes as a Metal-Free Heterogeneous Catalyst for Mild CO_2 Reduction to Methanol with Hydroboranes

Giulia Tuci,[a] Andrea Rossin,[a] Lapo Luconi,[a] Cuong Pham-Huu,[b] Stefano Cicchi,[c] Housseinou Ba,[b] and Giuliano Giambastiani *,[a,c]*

[a] Institute of Chemistry of OrganoMetallic Compounds, ICCOM-CNR and Consorzio INSTM, Via Madonna del Piano, 10 – 50019, Sesto F.no, Florence, Italy. E-mail: giuliano.giambastiani@iccom.cnr.it

[b] Institut de Chimie et Procédés pour l'Energie, l'Environnement et la Santé (ICPEES), UMR 7515 CNRS - University of Strasbourg, 67087 Strasbourg Cedex 02, France.

[c] Dipartimento di Chimica "Ugo Schiff", Università di Firenze, 50019, Sesto Fiorentino, Italy.

[d] Kazan Federal University, 420008 Kazan, Russian Federation.

Contents:

Experimental section.

General Considerations and material characterizations. All reactions were performed under dry N_2 atmosphere using standard Schlenk-type techniques or in a glovebox filled with N_2. Nitrogen (> 99.999%; Rivoira) was dried through a $CaCl_2$ column and deoxygenated with an oxysorb cartridge from Messer Griesheim. Thf (tetrahydrofuran), *o*DCB (orthodichlorobenzene) were purified according to literature procedures[1] and stored over 4Å molecular sieves under nitrogen atmosphere. Acetonitrile was dried by means of an MBraun solvent purification system. Pristine MWCNTs (98% in C) were purchased from Sigma-Aldrich and used as received without any further purification. Unless otherwise stated, all other chemicals/solvents were purchased from commercial suppliers and used as received. N^{py}-MW sample was prepared according to the literature procedure and fully characterized to determine the nature and loading of the chemically grafted N-containing groups.[2] All characterization data (Figure S1 and Table S1) were fully consistent with those coming from the literature.[2] Samples sonication was carried out in a water/ice bath using an Elma S15 Elmasonic sonicator bath (37 kHz). *Thermogravimetric Analysis (TGA)*. Analyses were performed under air (100 mL/min) on an EXSTAR ThermoGravimetric Analyzer (TG/DTA). *X-ray Photoelectron Spectroscopy (XPS)*. Analyses were performed in an ultra-high vacuum system (10^{-9} mbar) equipped with a VSW HAC 5000 hemispherical electron energy analyzer and a non-monochromatized Mg-Kα X-ray source (1253.6 eV). The source power was 120 W (12 kV x 10 mA) and the spectra were acquired at 53° takeoff angle respect to the sample normal. Survey spectra were acquired at a pass energy of 44 eV with an energy step size of 1 eV. High resolution spectra of detected elements were recorded for detailed BE chemical shift analysis at a pass energy of 22 eV with a step size of 0.05 eV. Samples, in the form of powders, were fixed on vacuum compatible carbon adhesive tape ensuring, as much as possible, a uniform coverage and were kept in the introduction chamber for at least 12 h, allowing the removal of adsorbed volatile substances. No charge compensation was used and the spectra were corrected using the sp^2 graphitic component of the C 1s spectrum as internal reference (binding energy, BE = 284.6 eV). *Elemental analyses* were performed on a Thermo FlashEA 1112 Series analyzer. CHNS average values are calculated over three independent runs. *Acid-Base Titration* was performed following the same procedure previously described by us;[2] briefly, 5 mg of the N^{py}-MW were suspended in 7 mL of a standard HCl solution, sonicated for 30 min and maintained in the dark at r.t. under stirring for 48 h. Afterwards, the suspension was centrifugated and three aliquots of the supernatant solution were titrated with a standardized solution of NaOH. The pyridine content (N_{Py}%) was calculated as average value over three independent runs. *^1H, $^{13}C\{^1H\}$* and *^{13}C NMR* spectra were recorded on a

Bruker Avance 400 MHz instrument. Chemical shifts are reported in ppm (δ) relative to TMS, referenced to the chemical shifts of residual solvent resonances. *Computational details:* Density Functional Theory (DFT) calculations were performed using the *Gaussian09* program (revision C.01).[3] Model structures were optimized with a M06-2X functional[4] using a 6-31G** basis set on all atoms. IRC analysis[5] was performed, to find the two minima linked by the related transition structure. When IRC calculations failed to reach the minima, geometry optimizations from the initial phase of the IRC path were performed. Frequency calculations were made on all the optimized structures, to characterize the stationary points as minima or TSs, as well for the calculation of zero-point energies, enthalpies, entropies and gas phase Gibbs energies at 298 K. Evaluation of the solvent effects was performed through a continuum modeling of the reaction medium. Bulk solvent effects (thf, ε = 7.42) were expressed through the SMD Continuum Model,[6] with the same basis set used for the gas phase optimizations. Gibbs energy in solution was calculated according to the following simplified equation: $G_{thf} = G_{gas} + (E_{thf} - E_{gas})$.

Catalytic runs in J Young NMR tube with isotopically enriched $^{13}CO_2$. For an initial screening of N^{Py}-MW catalytic performance in the CO_2 reduction with various hydroboranes, reactions were run in a 3 mL J Young NMR tube, using thf-d_8 as solvent and isotopically enriched $^{13}CO_2$ as substrate. In a typical run, the tube was charged under nitrogen atmosphere with 3 mg of N^{py}-MW, 0.4 mmol of the selected hydroborane (HBpin, HBcat, 9-BBN) and 1 mL of thf-d_8 and sonicated in an ice bath for 10 minutes. Afterwards, the tube was rapidly evacuated and re-filled with $^{13}CO_2$ at the final pressure of 1 atm. The reaction course was then followed via ^{13}C and $^{13}C\{^1H\}$ NMR spectroscopy after keeping the mixture at room temperature for 24 h.

Catalytic runs with 9-BBN as reducing agent. *Otherwise stated, catalytic tests were run in a 60 mL stainless steel autoclave equipped with a glass sample holder and an inner Teflon lining used to reduce the reactor internal volume to 14 mL.* In a typical procedure, 4.5 mg of N^{py}-MW (corresponding to 0.005 mmol of N basic sites) are suspended in thf-d_8 (1.5 mL) using the glass sample holder and the resulting mixture is sonicated for 10 minutes in an ice/water bath under nitrogen atmosphere. The resulting homogeneous dispersion is treated in one portion with the dimeric hydroborane $(9\text{-BBN})_2$ under nitrogen atmosphere (0.22 g, 0.90 mmol, 3.2 eq. with respect to CO_2). Afterwards, the reactor (14 mL in volume) is filled with CO_2 (1 bar) and the reaction products are monitored at fixed times. After each run, the reactor is cooled in an ice bath and the crude reaction mixture is treated with dry CH_3CN as internal standard (30 μl, 0.57 mmol). After

stirring the mixture for few seconds, the suspension is gently flushed with nitrogen, transferred in a 3 mL J. Young NMR tube and analyzed overnight *via* $^{13}C\{^1H\}$ NMR spectroscopy (d1 = 28 s). Attempts to follow the reaction process via ^1H-NMR are limited by the very poor quality of the spectra acquired on the heterogeneous suspension. NMR signals (100 MHz, thf-d_8) recorded at δ_C = 86.5, 53.4 and 0.45 ppm are unambiguously attributed to boronic esters $H_2C(OBBN)_2$ (**2**),[7] CH_3OBBN (**3**)[7] and CH_3CN[8] (internal standard), respectively. For two of the most representative catalytic tests outlined in Table 2 (entries 3 and 5), the quantitative analysis based on $^{13}C\{^1H\}$ NMR spectroscopy using CH_3CN as internal standard has been confirmed on a second reaction batch *via* GC-MS analysis of the hydrolyzed esters, using EtOH (≥99,8%) as internal standard (Figure S7).
For the catalytic test carried out with the full reactor volume (60 mL; Table 2, entry 5), the experimental conditions used are identical to those outlined above (for the 14 mL reactor) except for the amount of solvent (2 mL of thf-d_8 + 4 mL of thf), that of $(9\text{-BBN})_2$ (3.6 mmol, 3.2 eq.) and the amount of CH_3CN as internal standard (120 µl, 2.28 mmol).

Recycling tests. For catalyst recycling tests, the N^{Py}-MW suspension is analyzed overnight *via* $^{13}C\{^1H\}$ NMR spectroscopy (d1 = 28 s) after each run, then it is transferred in a glass vial, diluted with thf (5 mL), sonicated for 5 minutes and centrifuged in order to recover the solid material. The washing procedure is repeated three times before drying the solid residue (Cat.) under vacuum at 40 °C to constant weight. Tests confirm that recycled N^{Py}-MW maintains almost unchanged its catalytic performance after 10 successive cycles (Figure S6).

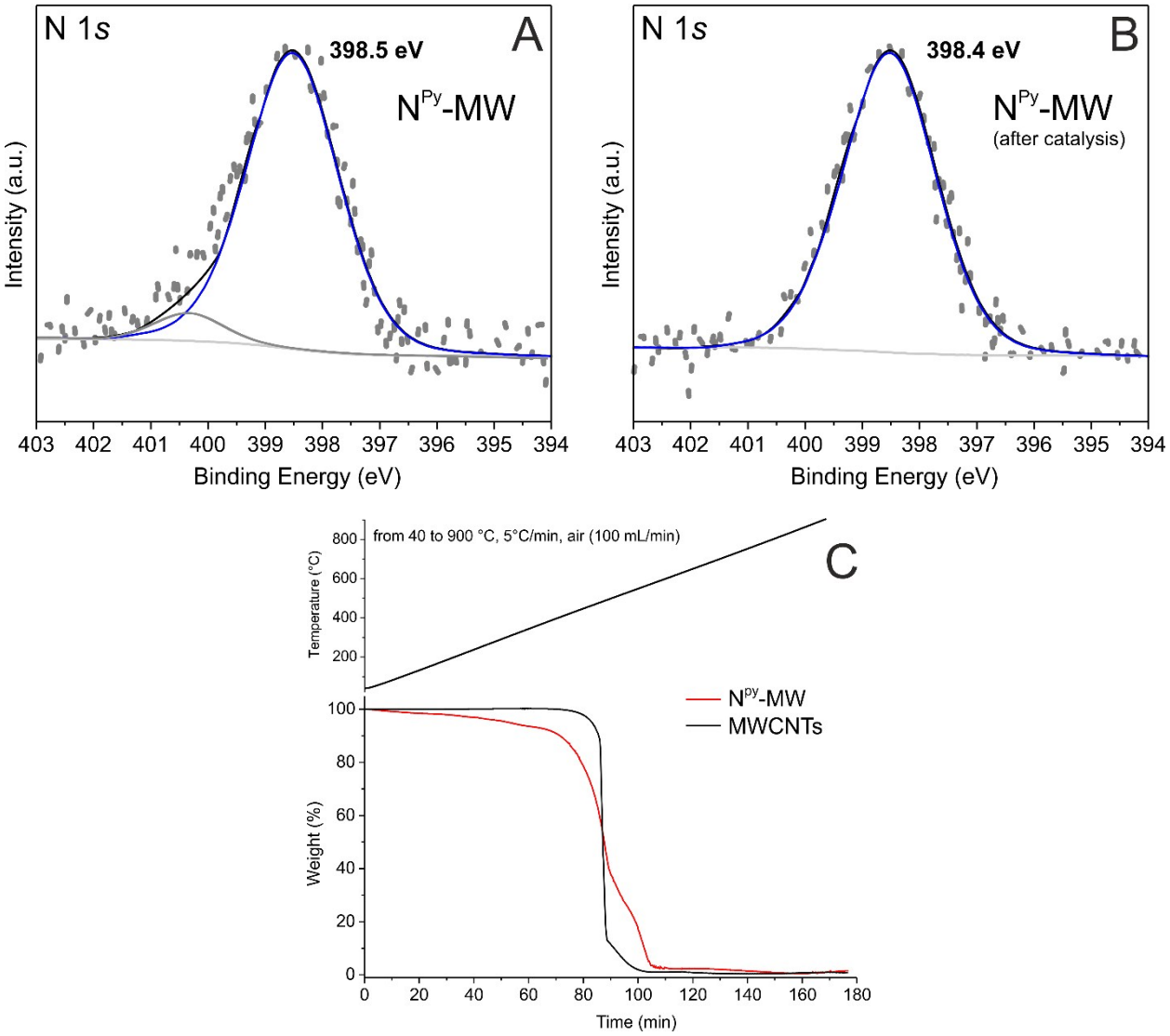

Figure S1. **A)**: N 1s XPS core region spectrum and its relative fit for the freshly prepared N^{Py}-MW. A minor component at higher binding energy is ascribed to commonly observed surface contaminations.[9] **B)**: N 1s XPS core region spectrum and its relative fit of the used N^{Py}-MW catalyst after 10 successive hydroboration runs (Table 2, entry 8). **C)**: TGA profiles of pristine MWCNTs (black-line) and N^{Py}-MW (red-line). Thermal program: 40-900 °C, 5°C/min; air atm., 100 mL min^{-1}.

	N_{py}% (*Elemental analyses*)	N_{py}% (*acid-base titration*)		N_{py}% on the used catalyst * (*Elemental analyses*)
N^{py}-MW $_{(1° run)}$	1.66	1.30		1.45
N^{py}-MW $_{(2° run)}$	1.43	1.58		1.57
N^{py}-MW $_{(3° run)}$	1.53	1.47		1.41
N^{py}-MW $_{(average)}$	**1.54**	**1.45**		**1.48**

Table S1. Elemental analyses and acid-base titrations on N^{Py}-MW sample for the determination of the N^{Py} loading. The N^{Py} content has been calculated as an average value over three independent runs. * Elemental analysis conducted on N^{Py}-MW after 10 successive catalytic runs (see Table 2, entry 8). The recovered catalyst was washed with ethylacetate and then twice with dichloromethane, each time sonicated for 10 min and separated from the supernatant by centrifugation. The solid residue

was finally suspended in dichloromethane and filtered through a 0,2 µm-pore PTFE filter. The collected material was dried at 50 °C under vacuum to constant weight before undergoing analysis.

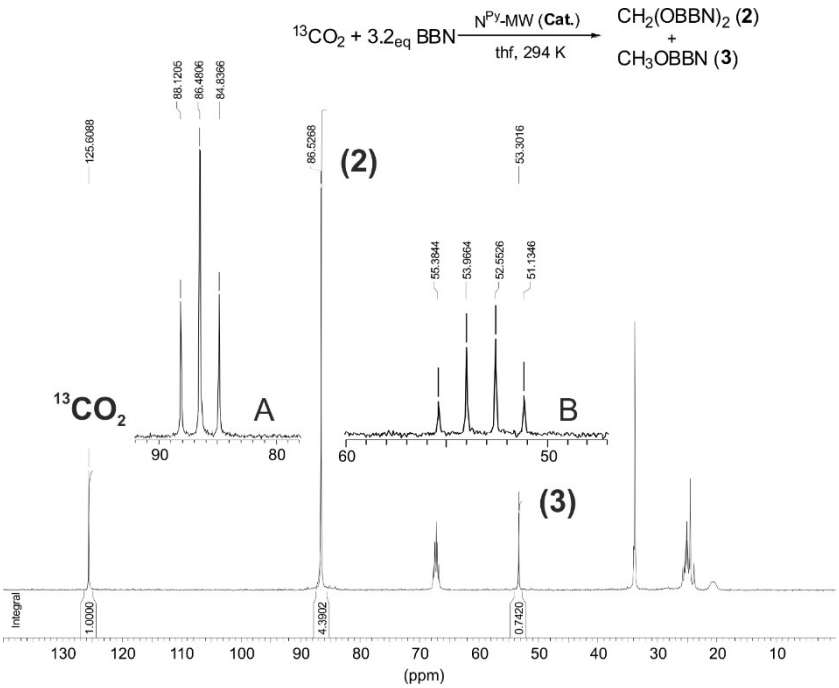

Figure S2. $^{13}C\{^1H\}$ NMR spectrum (100 MHz, thf-d_8, 294K, after 24h) of $^{13}CO_2$ (1 atm) hydroboration catalyzed by N^{Py}-MW using 3.2 eq. of 9-BBN as reducing agent. Insets A and B refer to the ^{13}C NMR spectra of products **2** (δ = 86.5 ppm) and **3** (δ = 53.3 ppm), respectively.

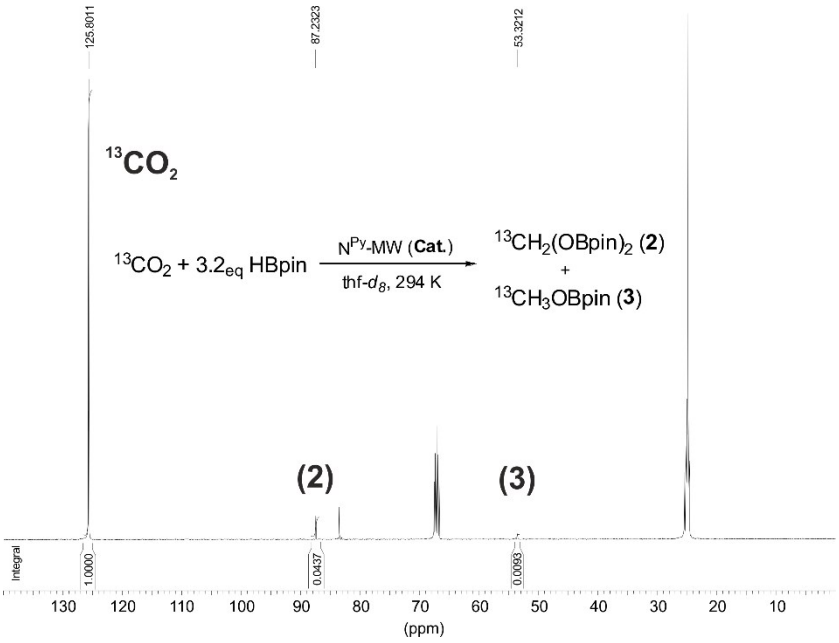

Figure S3. $^{13}C\{^1H\}$ NMR spectrum (100 MHz, thf-d_8, 294K, after 24h) of $^{13}CO_2$ (1 atm) hydroboration catalyzed by N^{Py}-MW using 3.2 eq. of HBpin as reducing agent.

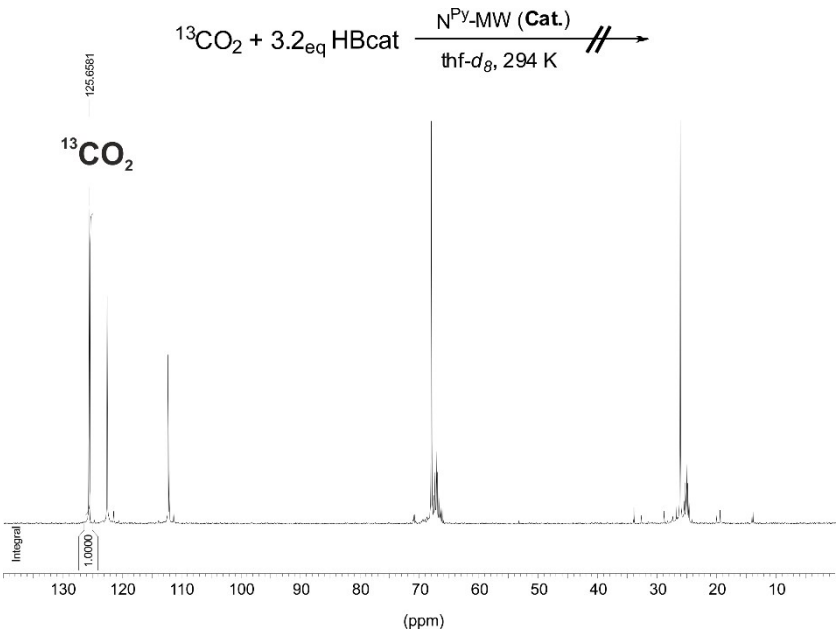

Figure S4. $^{13}C\{^1H\}$ NMR spectrum (100 MHz, thf-d_8, 294K, after 24h) of $^{13}CO_2$ (1 atm) hydroboration catalyzed by N^{Py}-MW using 3.2 eq. of HBcat as reducing agent.

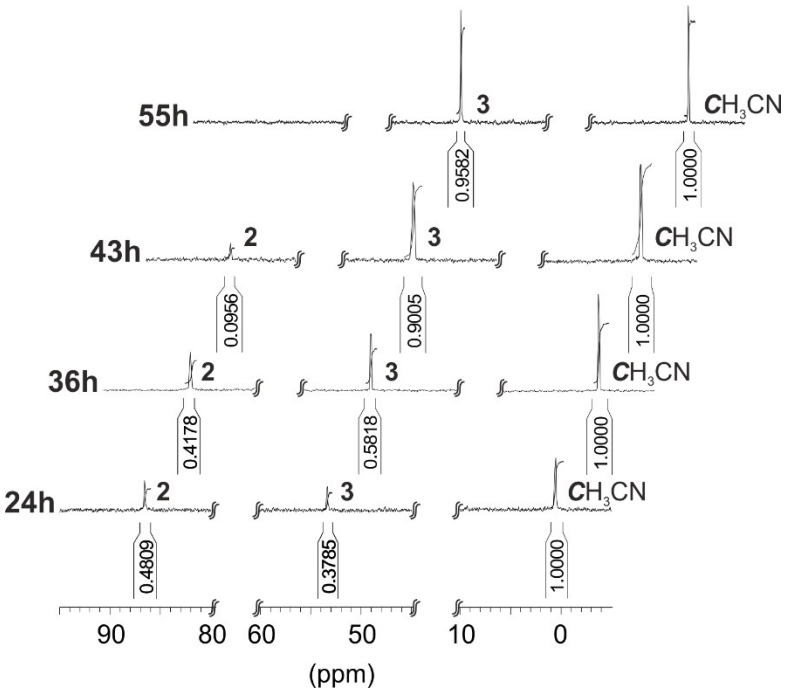

Figure S5. $^{13}C\{^1H\}$ NMR spectra (100 MHz, thf-d_8, 294K) at variable reaction times for the CO_2 hydroboration catalyzed by N^{Py}-MW with 3.2 eq. of 9-BBN as reducing agent. Quantitative estimation of $H_2C(OBBN)_2$ (**2**) and CH_3OBBN (**3**) is based on CH_3CN as internal standard (see experimental section). Data from the spectra above are graphically outlined on Figure 1.

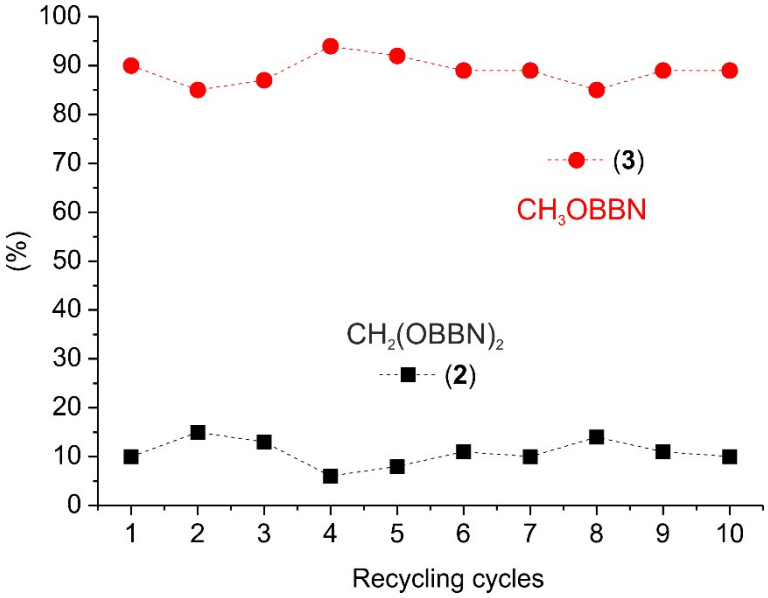

Figure S6. Recycling tests with N^{Py}-MW as catalyst in CO_2 hydroboration to boronic esters $H_2C(OBBN)_2$ (**2**) and CH_3OBBN (**3**) using 9-BBN as reducing agent. See also Table 2, entries 7 and 8 and experimental section for details.

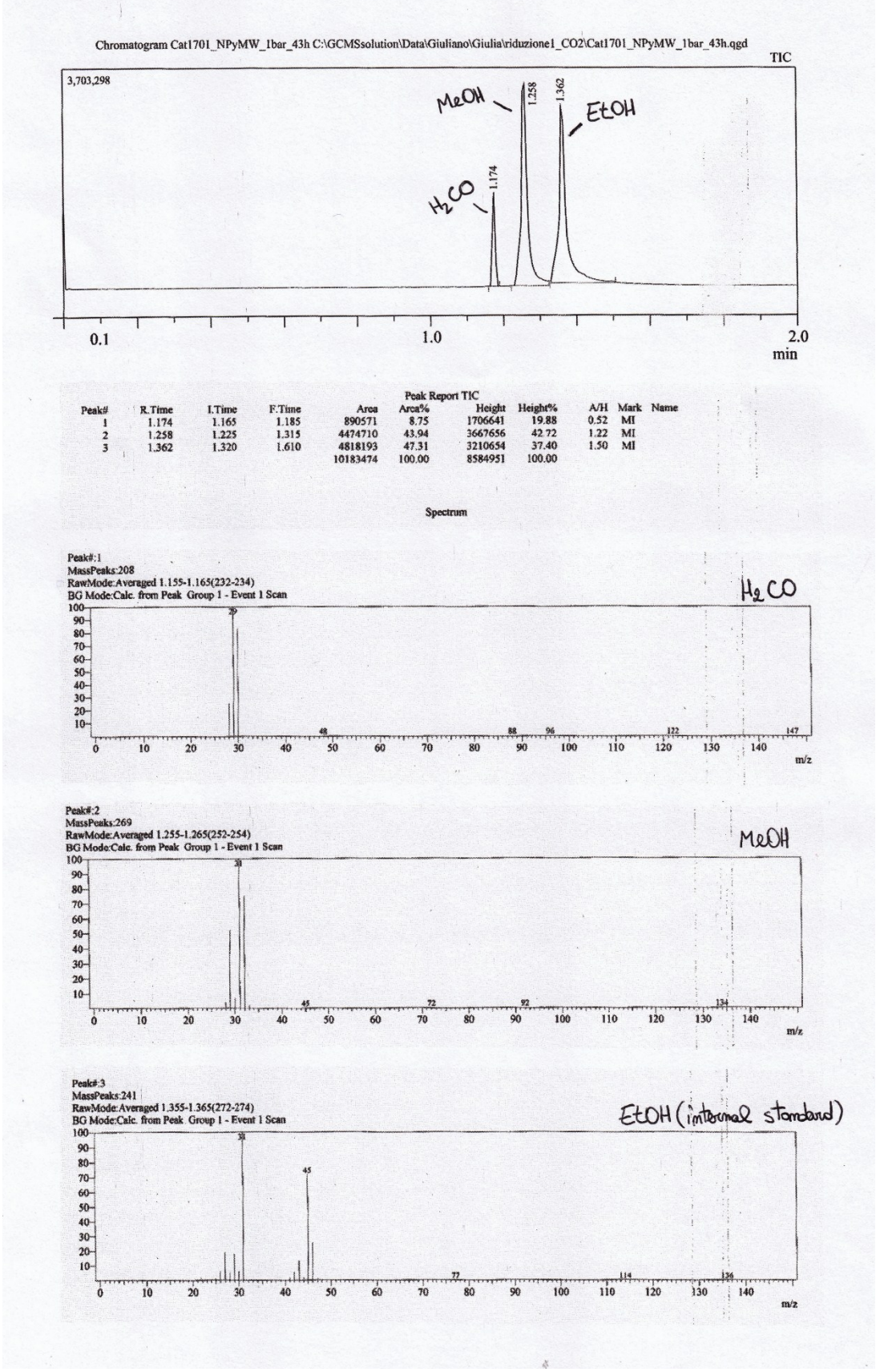

Figure S7. GC trace (after hydrolysis) of the CO_2 hydroboration reaction catalyzed by N^{Py}-MW using 3.2 eq. of 9-BBN as reducing agent (Table 2, entry 3) and MS spectra of each reaction product (GC program: 30°C/3min, 15°C/min, 250°C/20min).

Table S2. Catalytic performance of metal and metal-free systems of the *state-of-the-art* for the CO_2 hydroboration to methoxyborane **3**.

	Catalyst / (loading mol %) [a]	**P_{CO2} (atm)**	**Temp. (°C)**	**TON**	**TOF (h^{-1})**	**Ref.**	
Metal-Free catalyst	N^{Py}-MW / 0.3	1	21	**1141**	**11.9**	**this work**	Heterogeneous system
Transition & main group metal complexes	[P,C$^-$,P]NiH / 0.2	1	25	495	495	10	Homogeneous system
	[P,P,N,N$^-$]RuCl / 1	1	50	9	0.09	11	
	$[P]_2(H_2)_2RuH_2$ / 8	1	25	8[b]	0.8	12	
	$[P]_2(H_2)_2RuH_2$ / 10	1	25	1[b]	2	13	
	{[β-diketiminato]MgH}$_2$ / 10	1	60	10[b]	0.07	14	
	{[β-diketiminato]CaH}$_2$ / 10	1	60	10[b]	0.1	14	
	[β-diketiminato]GaH^{t}Bu / 10	1	60	10[b]	2.5	15	
	[Fe(PhSi{CH_2PPh_2})(MeCN)$_3$][OTf]$_2$ / 1.5	1	60	66	1.7	16	
	Co(PhSi{CH_2PPh_2}$_3$)Cl_2 / 1.5	1	60	66	1.7	16	
	[P,C$^-$,P]NiSR / 0.2	1	25	490	2400	17	
Metal-Free catalyst	1,5,7-triazabicyclo [4.4.0]dec-5-ene / 0.1	1	25	537	3.6	7	
	7-methyl-1,5,7-triazabicyclo [4.4.0]dec-5-ene / 0.1	1	25	648	33	7	
	2,8,9-trimethyl-2,5,8,9-tetraaza-1-phosphabicyclo[3.3.3]undecane / 0.01	1	20	6043	33	18	
	2,5,8,9-tetraaza-1-phosphabicyclo[3.3.3]undecane/ 0.5	1	70	100	287	18	
	$^tBu_3P$ /0.02	5	60	5556	176	19	
	Ferrocene, phosphino-boranes derivative (3-$BMes_2$) / 1	1	70	1980	99	20	
	[1,5,7-triazabicyclo[4.4.0]dec-5-ene]$SiMe_2Cl$ / 2.5	1	20	24	3.7	21	
	N-heterocyclic carbene (*a*NHC) dicarboxylate / 0.005	1	25	6000	500	22	
	Phosphine-borane (PB) adduct with CH_2O / 0.2	2	70	1005	670	23	

[a] mol % calculated respect to borane. [b] estimated from catalytic data reported on the original paper

Computational study. 9-BBN weakly interacts with carbon dioxide [optimized d(B−O) = 2.62 Å], forming an adduct [9-BBN···CO_2] lying 4.8 kcal mol^{-1} above the isolated reagents. The reaction is carried out in thf; in this solvent, the borane is present as a thf adduct [9-BBN···thf]. A preliminary thf replacement by CO_2 is therefore necessary for the formation of [9-BBN···CO_2]. The thermodynamics of the reaction [9-BBN···thf] + CO_2 → [9-BBN···CO_2] + thf is uphill: ΔG = +13.4 kcal mol^{-1}. The [9-BBN···CO_2] adduct was then put together with [9-BBN···Py], and the ensemble re-optimized without restrictions. The obtained geometry is the starting point for the successive Transition State search for the hydroboration reaction. In this structure, CO_2 simultaneously interacts with the B−H bond of one borane molecule through its carbon atom [optimized d(O_2C···H−B) = 2.56 Å] and with the boron atom of the second borane molecule through an oxygen atom [optimized d(O=C=O···B) = 2.50 Å]. From here, a Transition State **TS$_1$** for the first reduction to a (bridging) formate species was found, lying at 13.3 kcal mol^{-1} above the starting geometry (Figure S8). The product contains a bridging formate molecule between two B atoms (**1**→N_{Py}). The thermodynamics is strongly favored in thf: ΔG = − 30.5 kcal mol^{-1}.

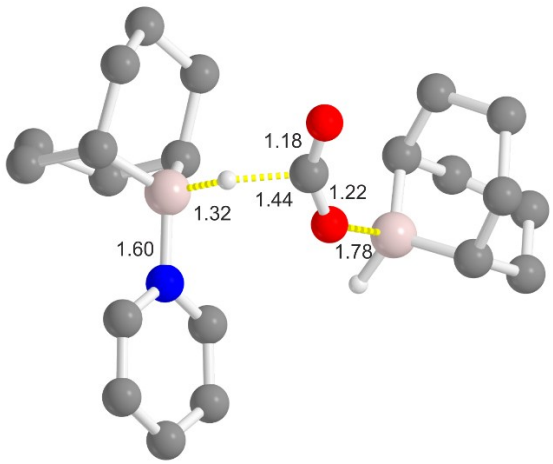

Figure S8. Optimized structure of **TS$_1$**. Selected optimized bond lengths reported (Å). H atoms on 9-BBN and pyridine omitted for clarity. Atom color code: white, H; gray, C; blue, N; pink, B; red, O.

The second reduction step is intramolecular; from the first step intermediate **1**→N_{Py}, an internal hydrogen transfer from the borane molecule to the formate carbon atom is conceived. The related Transition State **TS$_2$** (Figure S9) provides a $\Delta G^{\#}$ value of 13.9 kcal mol^{-1}. The second reduction

product features a bridging formaldehyde fragment μ-OCH_2O (**2**→N_{Py}). The thermodynamics is again strongly favored in thf: $\Delta G = -19.5$ kcal mol^{-1}.

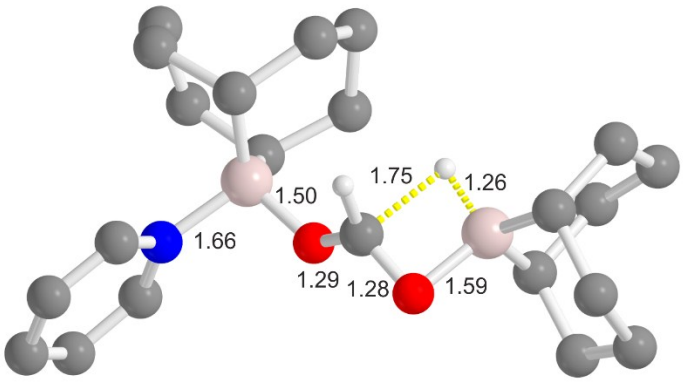

Figure S9. Optimized structure of $\mathbf{TS_2}$. Selected optimized bond lengths reported (Å). H atoms on 9-BBN and pyridine omitted for clarity. Atom color code: white, H; gray, C; blue, N; pink, B; red, O.

In the final stage, a third 9-BBN molecule is added to the previous model, and the ensemble re-optimized again. For this step, the thermodynamics Gibbs energy variation has been evaluated ($\Delta G = -35.4$ kcal mol^{-1}) to get the final products **3**→N_{Py} and the boronic ester R_2B-O-BR_2. Scheme S1 reports the Gibbs energy *vs.* reaction coordinate profile for the CO_2 to methanol transformation. The highest barrier to overcome to start the process equals 26.7 kcal mol^{-1} {$\Delta G^{\#}(\mathbf{TS_1}) + \Delta G$ for the preliminary [9-BBN···CO_2] formation}. Every step is thermodynamically downhill, in line with the experimental evidence. Given the almost identical values of $\Delta G^{\#}(\mathbf{TS_1})$ and $\Delta G^{\#}(\mathbf{TS_2})$, the first and second reduction steps occur simultaneously; this justifies the absence of the formate intermediate in the $^{13}C\{^1H\}$ NMR spectrum of the reaction mixture observed experimentally.

Finally, the influence of the carbon nanotube as an electron-donating support[24] for grafted pyridine groups has been simulated in the homogenous process through the insertion of a negative charge in the computational model, varying the total charge from 0 to −1. Following the same mechanistic scheme, the Transition State found for the first reduction step in the negatively charged system ($\mathbf{TS_1'}$, Figure S10) is found at a much lower energy than the corresponding $\mathbf{TS_1}$ for the neutral case. Indeed, a $\Delta G^{\#}$ value of only 7.5 kcal mol^{-1} is calculated for $\mathbf{TS_1'}$. In addition, the thermodynamics is much more favorable for the ionic system: $\Delta G = -42.0$ kcal mol^{-1}. This is in accordance with the experimental evidence of the activity of the N^{Py}-MW catalyst in CO_2 hydroboration.

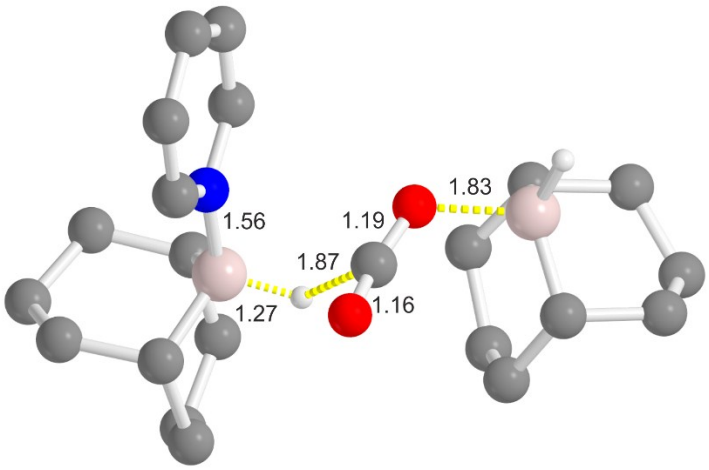

Figure S10. Optimized structure of **TS$_1$'**. Selected optimized bond lengths reported (Å). H atoms on 9-BBN and pyridine omitted for clarity. Atom color code: white, H; gray, C; blue, N; pink, B; red, O.

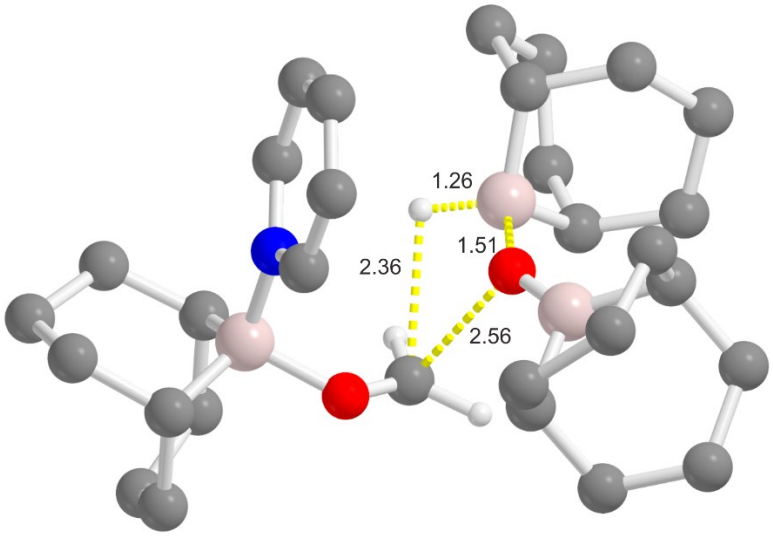

Figure S11. Optimized structure of **TS$_3$**. Selected optimized bond lengths reported (Å). H atoms on 9-BBN and pyridine omitted for clarity. Atom color code: white, H; gray, C; blue, N; pink, B; red, O.

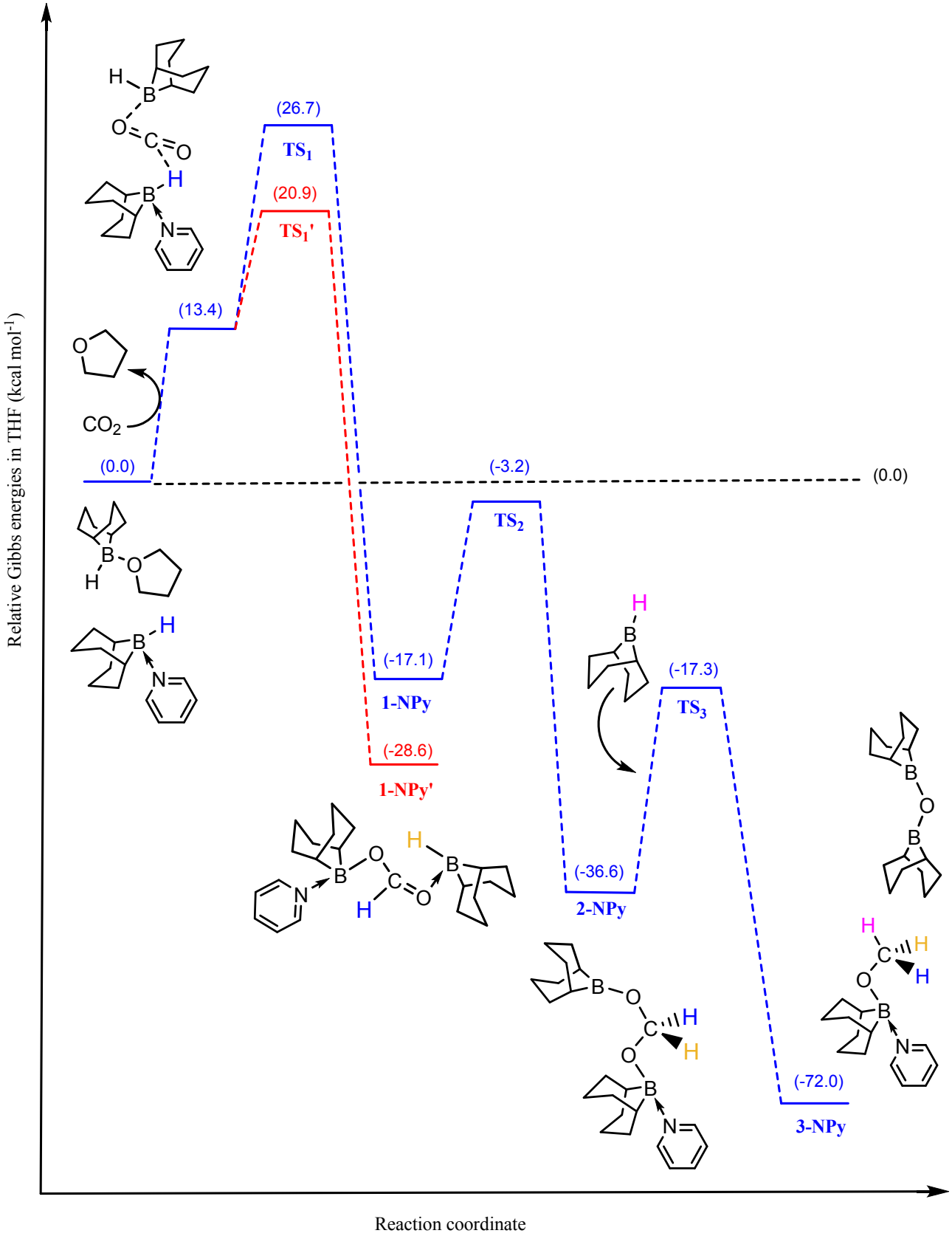

Scheme S1. Gibbs energy (thf) *vs.* reaction coordinate profile for the pyridine-catalyzed CO_2 reduction to methanol using 9-BBN as reducing agent. The zero charge and the negatively charged profiles are depicted with a blue and a red line, respectively.

Table S3. Mulliken atomic charges (q_i, e units) on the most relevant atoms (depicted in red in the Scheme) of the model reagent for the neutral and negatively charged systems studied in this work.

	Neutral system (n = 0)				**Charged system (n = −1)**			
	q_C	q_N	q_B	q_H	q_C	q_N	q_B	q_H
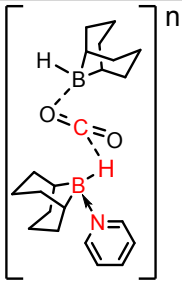	+0.71	−0.41	+0.34	-0.13	+0.71	−0.48	+0.43	-0.25
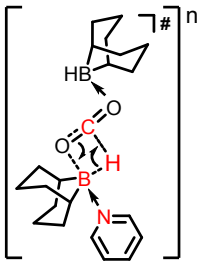	+0.63	-0.45	+0.39	-0.10	+0.71	-0.49	+0.44	-0.23
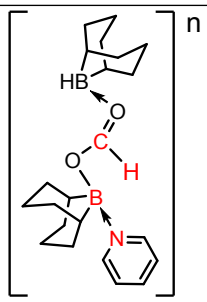	+0.47	-0.44	+0.62	+0.13	+0.48	-0.48	+0.64	+0.02

Optimized geometries of the DFT model structures (Cartesian coordinates plus absolute Gibbs energy values in thf).

TS_1

G_{thf} = –1113.402732 ha; ν = –213 cm^{-1}

C	3.057148	-1.745298	-0.242478
C	2.588237	-0.807994	0.888669
C	3.448133	1.248557	-0.461141
C	3.814232	0.314118	-1.629159
H	3.479436	-2.666871	0.183541
H	2.987144	0.337739	-2.352121
C	3.678141	-0.548867	1.956688

H	4.004218	-1.498515	2.402950
C	4.577895	1.445499	0.579063
H	5.495213	1.797389	0.086334
H	1.751656	-1.304267	1.403431
H	3.226987	2.238327	-0.884267
H	1.690912	1.396572	1.170659
C	4.075699	-1.149254	-1.235319
H	5.084802	-1.235581	-0.825366
H	4.078100	-1.763957	-2.143257
C	4.912413	0.208146	1.435477
H	4.263862	2.251951	1.255806
H	3.226547	0.036823	2.769091
H	4.693625	0.694718	-2.167795
H	2.177475	-2.067435	-0.813200
B	2.223790	0.657214	0.368653
H	5.521473	0.525389	2.290641
H	5.545178	-0.477517	0.867265
C	0.400849	-0.276988	-1.532839
O	0.856156	0.551895	-0.767940
O	0.570556	-1.051884	-2.406418
C	-2.451525	-0.848415	2.073795
C	-1.354369	-0.957027	0.990902
C	-3.204379	-0.986453	-0.849431
C	-4.287838	-0.920356	0.251580
H	-2.134632	-1.369623	2.986094
H	-4.635127	0.121172	0.331342
C	-0.971986	-2.405351	0.622087
H	-0.675614	-2.955126	1.525056
C	-2.765154	-2.416286	-1.234970
H	-3.631579	-2.993824	-1.582769
H	-0.440813	-0.503245	1.400768
H	-3.636862	-0.555441	-1.764348

H	-1.024248	-0.263310	-1.295514
C	-3.833496	-1.375792	1.649822
H	-3.839118	-2.465835	1.702460
H	-4.577710	-1.046234	2.384229
C	-2.048580	-3.207289	-0.128785
H	-2.084403	-2.328983	-2.092217
H	-0.071697	-2.363176	-0.006781
H	-5.167340	-1.505569	-0.047800
H	-2.555143	0.210808	2.354722
B	-1.903579	-0.220709	-0.317316
H	-1.577447	-4.087408	-0.580428
H	-2.781750	-3.603004	0.577819
C	-1.177379	2.044036	0.614272
C	-1.228090	3.425112	0.724799
C	-2.203277	4.125265	0.026783
C	-3.100424	3.417399	-0.769531
C	-2.989708	2.041293	-0.841447
N	-2.044678	1.366550	-0.159489
H	-2.265104	5.206086	0.097852
H	-0.420719	1.459456	1.121316
H	-0.498823	3.927011	1.348736
H	-3.877934	3.919176	-1.332228
H	-3.651823	1.439524	-1.450447

TS_2

G_{thf} = –1113.450409 ha; ν = –237 cm^{-1}

C	-4.456916	-1.604439	-1.117604
C	-3.607901	-0.336338	-1.340680

C	-2.924072	-0.382950	1.194620
C	-3.795159	-1.641733	1.387449
H	-5.344593	-1.600761	-1.766078
H	-3.121470	-2.507478	1.341260
C	-4.347139	0.994968	-1.096814
H	-5.243497	1.066235	-1.729298
C	-3.658498	0.955025	1.404710
H	-4.102408	1.007522	2.409103
H	-3.274339	-0.343965	-2.388914
H	-2.100903	-0.436031	1.922328
H	-1.576525	0.546357	-0.487896
C	-4.904390	-1.841682	0.336953
H	-5.757699	-1.200181	0.570401
H	-5.284711	-2.867263	0.422598
C	-4.750916	1.268725	0.364759
H	-2.903605	1.754602	1.360397
H	-3.677027	1.804402	-1.421432
H	-4.248970	-1.653284	2.388995
H	-3.846759	-2.461854	-1.431616
B	-2.391911	-0.404501	-0.310775
H	-5.031442	2.325351	0.457684
H	-5.657800	0.710182	0.607473
C	-0.496119	-0.804578	-0.746969
O	-1.444265	-1.651213	-0.564924
O	0.429050	-0.665651	0.143263
C	3.063962	1.962071	1.307471
C	1.729944	1.190990	1.289374
C	1.786425	1.153369	-1.306082
C	3.178586	1.822423	-1.265641
H	3.070525	2.697869	2.122665
H	3.961370	1.052137	-1.327947
C	0.471739	2.084271	1.239661

H	0.447083	2.749910	2.112237
C	0.648699	2.204906	-1.353858
H	0.886991	2.953395	-2.122024
H	1.647580	0.636870	2.237147
H	1.721929	0.606947	-2.261877
H	-0.289568	-0.422926	-1.754845
C	3.427985	2.670346	-0.009632
H	2.872861	3.606801	-0.095030
H	4.484989	2.959342	0.021146
C	0.327620	2.935703	-0.031855
H	-0.267870	1.716083	-1.700215
H	-0.402738	1.426328	1.330698
H	3.311843	2.455251	-2.152802
H	3.872916	1.252955	1.542041
B	1.635292	0.224302	0.009986
H	-0.703568	3.304245	-0.087232
H	0.950256	3.829396	0.059243
C	3.257440	-1.417332	1.214342
C	4.177662	-2.451690	1.288507
C	4.659639	-3.008861	0.109919
C	4.197889	-2.513788	-1.105483
C	3.278640	-1.477775	-1.099056
N	2.824989	-0.935671	0.040741
H	5.380294	-3.819385	0.137380
H	2.840428	-0.951192	2.098157
H	4.502230	-2.808432	2.258223
H	4.539910	-2.919275	-2.049795
H	2.883450	-1.054321	-2.014657

TS_1'

G_{thf} = –1113.478228 ha; ν = –307 cm^{-1}

C	2.788119	-1.158257	1.177937
C	3.452574	0.231192	1.249327
C	3.104463	0.520525	-1.317241
C	2.342377	-0.816314	-1.354842
H	3.303508	-1.858200	1.853112
H	1.269042	-0.589225	-1.294332
C	4.983377	0.191233	1.024291
H	5.463320	-0.453567	1.774899
C	4.632712	0.396748	-1.529970
H	4.850041	-0.138343	-2.466087
H	3.290451	0.629035	2.261971
H	2.716201	1.148441	-2.130422
H	3.239353	2.386983	0.206204
C	2.696675	-1.795523	-0.222376
H	3.634596	-2.305047	-0.461765
H	1.936907	-2.586422	-0.188363
C	5.407062	-0.277005	-0.379232
H	5.032557	1.412481	-1.656191
H	5.377633	1.203954	1.186399
H	2.496030	-1.325395	-2.317992
H	1.767304	-1.076710	1.575063
B	2.947425	1.223230	0.102603
H	6.478953	-0.078354	-0.510614
H	5.303066	-1.362786	-0.444715
C	0.507256	1.033765	1.235965
O	1.133501	1.392824	0.286792
O	0.083591	0.967929	2.316677
C	-3.904613	-1.130493	0.829420
C	-2.413074	-1.105823	1.221102
C	-1.760171	-1.189814	-1.292165

C	-3.251390	-1.142643	-1.674745
H	-4.493448	-1.714558	1.555325
H	-3.503710	-0.095408	-1.891962
C	-1.791212	-2.500292	1.418385
H	-2.331967	-3.068216	2.192169
C	-1.201412	-2.609986	-1.094507
H	-1.388826	-3.233590	-1.983302
H	-2.341602	-0.607385	2.200350
H	-1.202058	-0.767386	-2.142080
H	-0.330660	-0.419308	0.405159
C	-4.208882	-1.657036	-0.586012
H	-4.203453	-2.751001	-0.585032
H	-5.236425	-1.374708	-0.853211
C	-1.707595	-3.363180	0.148913
H	-0.110109	-2.515104	-1.011761
H	-0.771295	-2.349948	1.801188
H	-3.441720	-1.707029	-2.601753
H	-4.281447	-0.100371	0.888472
B	-1.555281	-0.331350	0.078764
H	-1.042365	-4.216375	0.341680
H	-2.687289	-3.804950	-0.056203
C	-2.565160	1.923186	0.906359
C	-2.869739	3.246513	0.762358
C	-2.546015	3.952131	-0.424483
C	-1.862367	3.204289	-1.416479
C	-1.574707	1.882578	-1.234492
N	-1.933473	1.177435	-0.086209
H	-2.781373	5.000653	-0.554003
H	-2.791366	1.384774	1.817870
H	-3.365710	3.747339	1.589473
H	-1.541114	3.672562	-2.342933
H	-1.025829	1.310930	-1.972826

TS_3

G_{thf} = –1451.852956 ha; ν = –210 cm^{-1}

C	3.794666	-1.902274	1.349161
C	3.615684	-1.119749	0.026396
C	1.482232	-2.534110	-0.459467
C	1.801080	-3.437210	0.754492
H	4.856048	-1.943776	1.629025
H	1.106097	-3.156358	1.559252
C	4.306623	-1.779484	-1.191380
H	5.361439	-1.984268	-0.959708
C	2.124321	-3.018684	-1.778870
H	1.740406	-4.010279	-2.056907
H	4.076327	-0.136562	0.157277
H	0.391781	-2.532612	-0.602168
H	0.072472	-0.404298	-2.302076
C	3.233429	-3.331306	1.317494
H	3.910823	-3.968225	0.744446
H	3.242028	-3.743788	2.333963
C	3.657548	-3.062163	-1.746214
H	1.812943	-2.337213	-2.586622
H	4.318048	-1.034916	-1.998845
H	1.581046	-4.489847	0.524235
H	3.290772	-1.339190	2.150209
B	2.039615	-1.054843	-0.197109
H	4.032171	-3.233804	-2.762241
H	3.976039	-3.934460	-1.171038
C	-0.795013	-0.007652	-1.776585
O	1.202815	-0.016532	-0.172692
O	-1.481114	-0.799223	-1.119568

C	-4.753309	-1.251705	0.981128
C	-3.666609	-1.593084	-0.056513
C	-3.458734	0.927115	-0.669180
C	-4.606278	1.241171	0.324928
H	-5.474770	-2.074171	1.065177
H	-4.176561	1.634394	1.254995
C	-4.200998	-1.882998	-1.476246
H	-4.946540	-2.687838	-1.441651
C	-3.989557	0.623300	-2.090450
H	-4.599580	1.464674	-2.442317
H	-3.173165	-2.517035	0.279728
H	-2.841316	1.836789	-0.747108
H	-1.076796	1.038632	-1.886170
C	-5.511974	0.054458	0.701408
H	-6.255478	-0.112670	-0.079498
H	-6.087770	0.328133	1.592746
C	-4.802368	-0.677240	-2.221108
H	-3.140880	0.569481	-2.786060
H	-3.362998	-2.273230	-2.068815
H	-5.226688	2.051705	-0.078547
H	-4.271138	-1.170535	1.966556
B	-2.651258	-0.360742	-0.152881
H	-4.888546	-0.929386	-3.284097
H	-5.826099	-0.502893	-1.885410
C	-1.165818	-1.220956	1.722761
C	-0.403534	-1.118890	2.871242
C	-0.274251	0.123701	3.483882
C	-0.895531	1.226028	2.913168
C	-1.630737	1.054510	1.752044
N	-1.792315	-0.155363	1.189714
H	0.319808	0.232624	4.385237
H	-1.289933	-2.160272	1.196704

H	0.080778	-2.001469	3.270151
H	-0.790427	2.219881	3.330327
H	-2.102157	1.886195	1.248878
C	3.216762	2.321130	1.003007
C	1.677762	2.347362	1.013953
C	1.637170	2.157715	-1.574211
C	3.169078	2.031614	-1.589457
H	3.620492	3.029744	1.742713
H	3.403459	0.961777	-1.667382
C	1.096404	3.769482	0.915392
H	1.466163	4.407666	1.732383
C	1.110844	3.602796	-1.662779
H	1.509570	4.118419	-2.549002
H	1.375335	1.940048	1.990387
H	1.281253	1.640666	-2.485156
H	-0.200089	1.656099	-0.211238
C	3.890612	2.605357	-0.355809
H	4.009484	3.684784	-0.483749
H	4.914371	2.208530	-0.331780
C	1.380847	4.472909	-0.422078
H	0.019929	3.550174	-1.803590
H	0.003951	3.701690	1.042650
H	3.597838	2.497885	-2.489083
H	3.525413	1.328776	1.351631
B	1.046501	1.490486	-0.213912
H	0.772473	5.384011	-0.486527
H	2.418357	4.818541	-0.432925

References.

1. D. D. Perrin, W. L. F. Armarego and D. R. Perrin, *Purification of Laboratory Chemicals*, Pergamon, New York, 2nd ed. edn., 1980.
2. G. Tuci, C. Zafferoni, P. D'Ambrosio, S. Caporali, M. Ceppatelli, A. Rossin, T. Tsoufis, M. Innocenti and G. Giambastiani, *ACS Catal.*, 2013, **3**, 2108-2111.
3. M. J. Frisch and et al., 2010.
4. Y. Zhao and D. G. Truhlar, *Theor. Chem. Account*, 2008, **120**, 215-241.
5. K. Fukui, *Acc. Chem. Res.*, 1981, **16**, 363-368.
6. A. V. Marenich, C. J. Cramer and D. G. Truhlar, *J. Phys. Chem. B*, 2009, **113**, 6378-6396.
7. C. Das Neves Gomes, E. Blondiaux, P. Thuéry and T. Cantat, *Chem. Eur. J.*, 2014, **20**, 7098–7106.
8. G. R. Fulmer, A. J. M. Miller, N. H. Sherden, H. E. Gottlieb, A. Nudelman, B. M. Stoltz, J. E. Bercaw and K. I. Goldberg, *Organometallics*, 2010, **29**, 2176–2179.
9. (a) C. A. Dyke, M. P. Stewart, F. Maya and J. M. Tour, *Synlett*, 2004, **1**, 155-160; (b) M. K. Daletoua, F. Paloukisa and A. Stefopoulosa, *ECS Trans.*, 2009, **25**, 1915-1924; (c) B. K. Price and J. M. Tour, *J. Am. Chem. Soc.*, 2006, **128**, 12899-12904.
10. S. Chakraborty, J. Zhang, J. A. Krause and H. Guan, *J. Am. Chem. Soc.*, 2010, **132**, 8872–8873.
11. M. J. Sgro and D. W. Stephan, *Angew. Chem. Int. Ed.*, 2012, **51**, 11343 –11345.
12. S. Bontemps, L. Vendier and S. Sabo-Etienne, *Angew. Chem. Int. Ed.*, 2012, **51**, 1671–1674.
13. S. Bontemps, L. Vendier and S. Sabo-Etienne, *J. Am. Chem. Soc.*, 2014, **136**, 4419-4425.
14. M. D. Anker, M. Arrowsmith, P. Bellham, M. S. Hill, G. Kociok-Kohn, D. J. Liptrot, M. F. Mahon. and C. Weetman, *Chem. Sci.*, 2014, **5**, 2826–2830.
15. J. A. B. Abdalla, I. M. Riddlestone, R. Tirfoin and S. Aldridge, *Angew. Chem. Int. Ed.*, 2015, **54**, 5098-5102.
16. A. Aloisi, J.-C. Berthet, C. Genre, P. Thuéry and T. Cantat, *Dalton Trans.*, 2016, **45**, 14774–14788.
17. T. Liu, W. Meng, Q.-Q. Ma, J. Zhang, H. Li, S. Li, Q. Zhao and X. Chen, *Dalton Trans.*, 2017, **46**, 4504-4509.
18. E. Blondiaux, J. Pouessel and T. Cantat, *Angew. Chem. Int. Ed.*, 2014, **53**, 12186 –12190.
19. T. Wang and D. W. Stephan, *Chem. Commun.*, 2014, **50**, 7007-7010.
20. A. Tlili, A. Voituriez, A. Marinetti, P. Thuéry and T. Cantat, *Chem. Commun.*, 2016, **52**, 7553-7555.
21. N. von Wolff, G. Lefèvre, J.-C. Berthet, P. Thuéry and T. Cantat, *ACS Catal.*, 2016, **6**, 4526−4535.
22. S. C. Sau, R. Bhattacharjee, P. K. Vardhanapu, G. Vijaykumar, A. Datta and S. K. Mandal, *Angew. Chem. Int. Ed.*, 2016, **55**, 15147–15151.
23. R. Declercq, G. Bouhadir, D. Bourissou, M.-A. Légaré, M.-A Courtemanche, K. S. Nahi, N. Bouchard, F.-G. Fontaine and L. Maron, *ACS Catal.*, 2015, **5**, 2513-2520.
24. C. Fantini, M. L. Usrey and M. S. Strano, *J. Phys. Chem. C*, 2007, **111**, 17941-17946.